Eur. J. Mineral., 36, 345–360, 2024
https://doi.org/10.5194/ejm-36-345-2024

European Journal of Mineralogy
Open Access

Metamorphic evolution of sillimanite gneiss in the high-pressure terrane of the Western Gneiss Region (Norway)

Ane K. Engvik and Johannes Jakob

Geological Survey of Norway, P.O. Box 6315 Torgarden, 7491 Trondheim, Norway

Correspondence: Ane K. Engvik (ane.engvik@ngu.no)

Received: 1 February 2023 – Revised: 9 February 2024 – Accepted: 13 February 2024 – Published: 27 March 2024

Abstract. Sillimanite-bearing gneisses in the Romsdal region of the Western Gneiss Region (south Norway) have been investigated to document the presence, formation, composition and petrological evolution of the sillimanite-bearing assemblages. Sillimanite is found in augen gneiss, as nodular gneiss, and in well-foliated sillimanite–mica gneiss. Lenses and layers of eclogite occur within the gneiss units. The sillimanite-bearing gneisses are heterogranular and dominated by quartz, plagioclase ($An_{29–41}$), K-feldspar and biotite (Mg# = 0.48–0.58; Ti = 0.16–0.36 a.p.f.u.), with variable amounts of white mica (Si = 6.1–6.3). K-feldspar occurs as porphyroclasts in augen gneiss, and garnet constitutes resorbed porphyroblasts. Garnet ($Alm_{46–56}Sps_{24–36}Prp_{10–20}Grs_{4–6}$; Mg# = 0.22–0.29) shows rimward-decreasing Mg#, together with a smaller grossular decrease and a marked spessartine increase up to Sps_{36}. The foliation is defined by crystal-preferred-orientation micas, elongation of shape-preferred-orientation coarse K-feldspar phenocrysts and a modal banding of phases. Sillimanite occurs as coarse orientation-parallel matrix porphyroblasts, as finer grains and as fibrolitic aggregates. Quartz constitutes coarser elongated grains and monomineralic rods. Pseudosection modelling suggests that the peak-metamorphic mineral assemblage of garnet–sillimanite–feldspar–biotite–quartz–ilmenite–liquid equilibrated at temperatures up to 750 °C and pressures of 0.6 GPa. Subsequent retrogression consumed garnet. Mineral replacement and melt crystallization involved sillimanite, white mica, K-feldspar and quartz. The results document a metamorphic retrogression of the sillimanite gneisses in accordance with the presence of remnants of eclogites and high-pressure granulites in this northwestern part of the Western Gneiss Region.

1 Introduction

The Al-silicate sillimanite is an index mineral commonly used to define the metamorphic grade. Sillimanite is known as a high-temperature mineral and is included in the Barrovian metamorphic concept (Barrow, 1912; Gillen, 1982). It is usually present in quartz- and mica-rich schists and gneisses. Mica-rich gneisses may exhibit a peculiar nodular fabric containing coarse white nuggets of concentrated sillimanite (e.g. Vernon, 1979; Munz et al., 1994). The presence of sillimanite often suggests a sedimentary rock origin (e.g. Spry et al., 2022), although other studies suggest that it can also originate in a granitoid environment (Nabelek, 1997; McLelland et al., 2002). In the case of the Cooma Complex (Australia) and the Adirondack Mountains (North America), Vernon (1979) and McLelland et al. (2002) attributed the sillimanite formation to alkali leaching by hydrothermal fluids. Spry et al. (2022) connected sillimanite rocks of Colorado (North America) to hydrothermal processes and used them as a field indicator for sulfide deposits.

Sillimanite gneisses occur in the northwestern part of the Western Gneiss Region (WGR), Norway (Fig. 1). In the Romsdal area, sillimanite is found locally in augen gneisses. In addition, nodular and foliated sillimanite gneisses occur in layers and patches within this eclogite-bearing gneiss unit. Walsh and Hacker (2004) estimated peak-metamorphic temperatures (T) and pressures (P) of 650–800 °C and P_{min} = 1.6–1.8 GPa from the eclogite mineral assemblages in the region. In the adjacent coastal areas, the preserved peak metamorphism is of high-pressure (HP) granulite fa-

cies recording $T > 900\,°C$ and pressures varying from 1.4 to 2.3 GPa. The HP-granulite metamorphism is interpreted as a decompression stage following eclogite-facies metamorphism (Larsen et al., 1998; Butler et al., 2013; Engvik et al., 2018; Holmberg et al., 2019).

This paper documents the formation of the sillimanite gneiss. By petrographic studies, we identify and describe the mineral replacements and reactions resulting in the observed sillimanite–white-mica–quartz assemblage and its fabric. Mineral chemistry and equilibrium assemblage diagrams are used to document its P–T stability and the metamorphic evolution. The results are discussed with respect to the metamorphic evolution of the sillimanite gneiss, its regional importance, and the relationship to the eclogites in this northwestern part of the WGR.

2 Geological setting

The WGR in the western part of south Norway (Fig. 1) is a large gneiss terrane of Proterozoic age (e.g. Tucker et al., 1987; Engvik et al., 2000; Austrheim et al., 2003; Walsh et al., 2007; Røhr et al., 2012). It is one of the world's largest eclogite-facies provinces and has experienced HP to ultrahigh-pressure (UHP) metamorphism during the Caledonian continent–continent collision in late Silurian to Early Devonian times (e.g. Smith, 1984; Griffin et al., 1985; Dobrzhinetskaya et al., 1995; Wain, 1997; Martin et al., 2010). The WGR is interpreted to represent the exhumed parts of the root zone of the Scandian orogen (e.g. Andersen et al., 1991; Engvik and Andersen, 2000; Roberts, 2003; Tucker et al., 2004; Hacker, 2007; Hacker et al., 2010; Walsh et al., 2013; DesOrmeau et al., 2015; March et al., 2022). P–T estimates reach 800 °C and 3.2 GPa, with the highest pressures and temperatures being reported from the northwestern part of the gneiss terrane (e.g. Krogh, 1977; Terry et al., 2000; Hacker et al., 2010). The presence of coesite inclusions in garnet and of diamond provides evidence for UHP metamorphism in the coastal part of the gneiss terrane (Smith, 1984; Dobrzhinetskaya et al., 1995; Wain, 1997; Vrijmoed et al., 2006; Butler et al., 2013).

3 Analytical methods

Samples were collected from drill cores through sillimanite-bearing gneisses from the Mannen transect in Romsdal (Saintot et al., 2011; Oppikofer et al., 2012; UTM32 coordinates 436619E, 6925616N; cores KH0110 and KH0211). Additional field investigations and sampling have been done in the Romsdal region to get a broader understanding of the structural and mineralogical relationships, exemplified by the localities Bispevatn (430313E, 6925570N) and Litjfjell (437757E, 6931462N). Petrography was studied on polished thin sections with both optical and scanning electron microscopy (SEM) using the LEO 1450 VP instrument at the Geological Survey of Norway (NGU). Quantitative mineral chemical data were collected along selected linear profiles through garnet crystals using an energy-dispersive spectrometer (EDS) mounted on the SEM. These analyses were performed at 10 nA sample current and 15 kV acceleration voltage. The counting time was 60 s live time.

For chemical characterization and pressure–temperature interpretation, minerals were analysed using a Cameca SX100 electron microprobe equipped with five wavelength-dispersive spectrometers (WDS) at the Institute of Geosciences, University of Oslo (Tables 1–3). The accelerating voltage was 15 kV and the counting time 10 s on peak using a beam current of 15 nA. A focused beam was used for garnet, but a beam diameter of 5 to 10 µm was used for analysing sheet silicates and plagioclase. Standardization was made on a selection of synthetic and natural minerals and oxides. Data reduction was done by the PAP program (Pouchou and Pichoir, 1984).

For the modelling of equilibrium assemblage diagrams, whole-rock major element analyses were carried out at NGU, measured on fused glass beads prepared by 1 : 7 dilution with lithium tetraborate (Table 4). The samples were analysed on a PANalytical Axios XRF spectrometer equipped with a 4 kW Rh X-ray tube, using common international standards for calibration.

4 Field relations of sillimanite gneisses in the Romsdal area

The northwestern part of WGR is dominated by migmatitic gneisses (Fig. 1b) of quartz-dioritic to granitic composition, partly as coarse-grained granitic augen gneiss (Tveten et al., 1998; NGU map database). Sillimanite-bearing gneisses are mapped following a zone crossing the WGR that extends from Sunndalen through Romsdal to Sunnmøre. These sillimanite-bearing gneisses are interlayered with a variety of eclogite-bearing gneisses. In the Romsdal area the K-feldspar phenocrysts that form the "augen" are prominent in wide parts of the area. Sillimanite-bearing rocks (Fig. 2) occur in zones and layers throughout the region, not only as thinner zones within the units mapped as sillimanite gneiss, but also in the units mapped as migmatites, granitic orthogneisses and augen gneisses (Fig. 1; Tveten et al., 1998; NGU map database).

Sillimanite is found in augen gneiss (Fig. 2a), constituting nuggets in so-called nodular gneiss (Fig. 2b–c), and present in well-foliated sillimanite–mica-rich gneiss (Fig. 2d). The gneisses are partly garnet bearing (Fig. 2e). In Romsdal, the gneisses vary from fine- to coarse-grained, exhibit well to strongly developed foliation, and contain feldspar–quartz leucosome pockets and pegmatites (Fig. 2f–g). Related garnet–mica gneiss occurs interlayered with the sillimanite-bearing horizons. Amphibolite and eclogite occur in minor amounts, also within the sillimanite-bearing units (Fig. 2h).

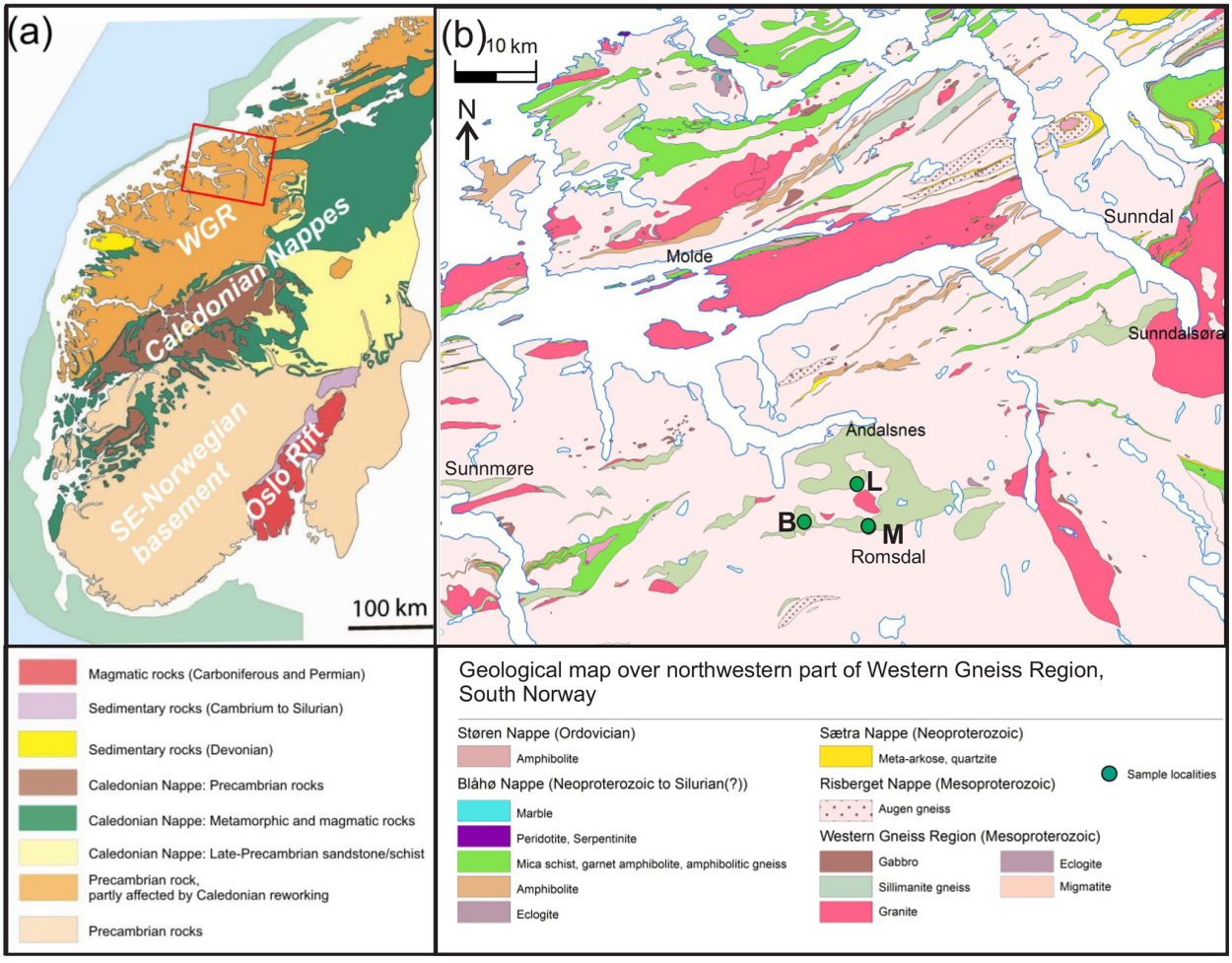

Figure 1. (a) Large-scale geological map of south Norway; square indicates area of panel **(b)**. **(b)** Geological map of the northwestern part of the Western Gneiss Region, south Norway (based on Engvik et al., 2018; compilation following Tveten et al., 1998, and NGU bedrock map database 1 : 250 000). Green-filled circle indicates sampled locality. M: Mannen locality; B: Bispevatn locality; L: Litjfjell locality.

In this region, U–Pb age dating of zircon and monazite reveals a wide range of Precambrian protolith ages (1700–950 Ma) from the granitic gneisses and migmatites, with a high-temperature metamorphic event of Caledonian age (470–395 Ma) (Walsh and Hacker, 2004; Walsh et al., 2007). However, up to date, no U–Pb zircon geochronological data have been published from the units mapped as sillimanite-bearing gneisses in Fig. 1.

5 Mineralogy, microfabric and mineral chemistry

The sillimanite-bearing gneiss units of the Romsdal area are dominated by quartz, plagioclase ($An_{29–41}$), K-feldspar and biotite with variable amounts of phengitic white mica (Si = 6.1–6.3). Biotite has Mg/(Mg+Fe) = 0.48–0.58 (Mg#) and Ti = 0.16–0.36 a.p.f.u., with the lowest Mg# in the core of coarser biotite grains. The gneisses are heterogranular with K-feldspar porphyroclasts (Fig. 3a), sillimanite (Fig. 3b) and, locally, garnet porphyroblasts (Fig. 3c). The K-feldspar porphyroclasts occur partly as perthite. Ilmenite, apatite, zircon and monazite occur as accessory phases.

Strongly foliated horizons are dominated by a fine-grained (< 0.5 mm) matrix of quartz, plagioclase, K-feldspar, and biotite, and a foliation is defined by the crystal-preferred orientation of micas, elongation of shape-oriented K-feldspar phenocrysts, and a modal banding of phases (Fig. 3a–b). The K-feldspar phenocrysts reach 2 cm in size (Figs. 2a; 3a) and occur with ellipsoidal foliation-parallel porphyroclasts and with a shape-preferred orientation including pressure shadows on the long-axis limb. Sillimanite occurs both as orientation-parallel matrix crystals and porphyroblasts up to 2 cm in length (Fig. 3a–b), as finer grains but dominantly as fibrolitic aggregates formed by very fine-grained needles fringing a sillimanite crystal (Fig. 3d). Quartz occurs also as coarser elongated grains (< 2 mm) and monomineralic rods (Fig. 3b). In samples rich in sillimanite and mica, the rock

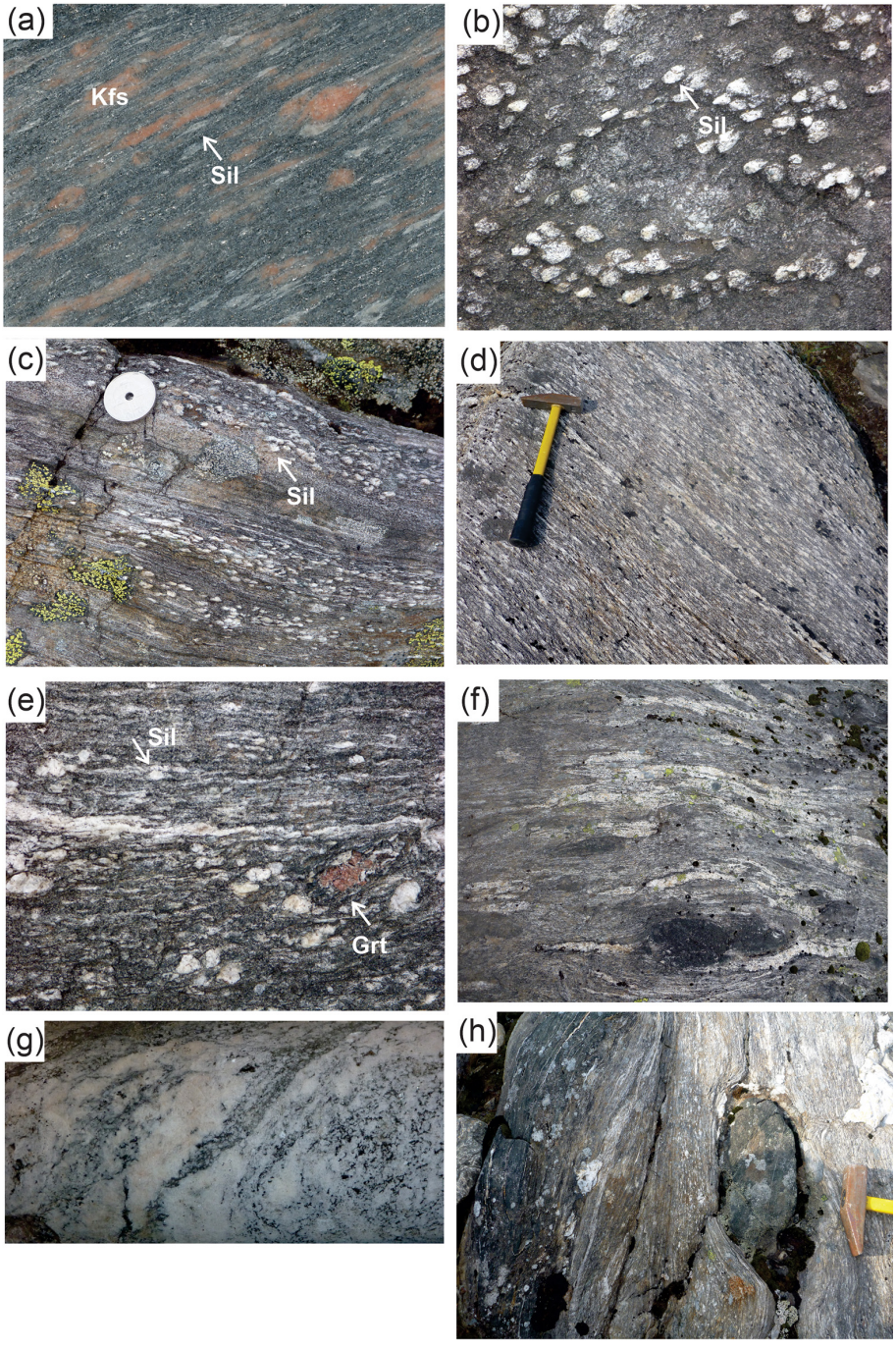

Figure 2. Field and drill core photographs. **(a)** Augen gneiss with pink K-feldspar porphyroclast (drill core sample, MAN3). Light-grey needles are sillimanite occurring around the K-feldspars and along gneiss foliation. **(b)** Nodular gneiss with the characteristic white nodules with sillimanite concentrations. Locality: Litjfjell, Romsdalen. Field of view is ca. 0.5 m wide. **(c)** Horizons with sillimanite nodules in foliated granitic to quartz-dioritic gneiss. Locality: Bispevatn, Romsdalen. **(d)** Strongly foliated sillimanite gneiss; flattened light spots include sillimanite. Locality: Bispevatn, Romsdalen. **(e)** Garnet-bearing sillimanite gneiss, including outcrop-visible red garnet (right part) and sillimanite included in the light spots. Locality: Bispevatn, Romsdalen. Field of view is ca. 0.2 m wide. **(f)** Foliation-parallel leucosome pockets (light horizons) in sillimanite-bearing gneiss unit. Locality: Bispevatn, Romsdalen. Field of view is ca. 1 m wide. **(g)** Leucosome melt pocket in foliated biotite gneiss (drill core KH0110; field of view is ca. 10 cm wide). **(h)** Inhomogeneous, foliated sillimanite gneiss including a dark amphibolite boudin. Locality: Bispevatn, Romsdalen.

Table 1. Representative electron-microprobe analyses of garnet (oxide wt %, formula in atoms per formula unit, a.p.f.u.).

Rock type	Grt-mica gneiss			Grt-Sil gneiss		Grt-mica gneiss
Sample no.	MAN2A	MAN2A	MAN2A	MAN3A	MAN3A	MAN4
Analysis no.	1	13	22	48	61	69
Comment	core	core	small, core	core	core	core
SiO_2	37.07	37.46	37.01	37.42	37.47	37.27
Al_2O_3	20.86	20.89	20.60	21.10	21.03	20.91
TiO_2	0.00	0.02	0.00	0.02	0.00	0.00
Cr_2O_3	0.01	0.00	0.05	0.02	0.00	0.00
FeO	24.37	24.76	23.22	25.50	23.69	23.63
MnO	9.07	7.34	11.89	10.77	12.92	10.98
MgO	3.00	3.00	2.77	4.20	3.73	2.43
CaO	5.49	6.46	3.74	1.61	1.88	5.15
Total	99.87	99.93	99.28	100.64	100.71	100.37
Formula based on eight cations						
Si	2.96	2.98	2.99	2.97	2.98	2.98
Al	1.97	1.96	1.96	1.97	1.97	1.97
Ti	0.00	0.00	0.00	0.00	0.00	0.00
Cr	0.00	0.00	0.00	0.00	0.00	0.00
Fe^{2+}	1.63	1.65	1.57	1.69	1.58	1.58
Mn	0.61	0.50	0.81	0.72	0.87	0.74
Mg	0.36	0.36	0.33	0.50	0.44	0.29
Ca	0.47	0.55	0.32	0.14	0.16	0.44
Oxygen	11.95	11.97	11.97	11.96	11.97	11.96
Alm	53.0	54.0	51.6	55.5	51.7	51.7
Prp	11.6	11.7	11.0	16.3	14.5	9.5
Grs	15.3	18.1	10.7	4.5	5.2	14.4
Sps	20.0	16.2	26.8	23.7	28.6	24.3
Mg#	0.18	0.18	0.18	0.23	0.22	0.16

is quartz-rich and the feldspar phase is dominated by plagioclase.

Garnet occurs as inclusion-rich porphyroblasts with irregular grain boundaries (Figs. 3c and 4). The inclusions are evenly distributed in the garnet and constituted by quartz and biotite. Garnet is surrounded by biotite, white mica and quartz along its rims. The porphyroblasts vary in size, up to 0.5 cm, and occur preferably in layers modally richer in biotite. The garnet in the sillimanite gneiss is almandine- and spessartine-rich ($Alm_{46–56}Sps_{24–36}Prp_{10–20}Grs_{4–6}$; Mg# = 0.22–0.29; Table 1). It shows zoning towards the rims with decreasing Mg# and a smaller decrease in grossular and marked increase in spessartine component up to Sps_{36} (Fig. 4; Table 1).

The K-feldspar porphyroclasts display replacement along the rims. The replacement textures occur both as a grain size reduction and replacement reactions. The fine-grained fabric involves quartz, biotite, white mica and sillimanite (Figs. 3a; 5a). Aggregates of symplectitic, very fine-grained, white mica and quartz occur as replacement after sillimanite (Fig. 5c–d). K-feldspar porphyroclasts also form medium-grained, monomineralic aggregates (Fig. 5e) and foliation-parallel layers of monomineralic fine-grained aggregates (Fig. 5f). These layers are typically < 0.5 mm thick and composed of K-feldspar subgrains < 0.1 mm in size. Foliation-parallel quartz rods occur as elongated < 0.2 mm thick layers in the sillimanite-bearing augen gneiss (Fig. 3b).

Garnet–mica gneiss occurs with similar microfabrics to the sillimanite-bearing horizons but is richer in biotite, which defines a well-developed foliation in the rock. Garnet in garnet–mica gneiss shows a similar chemistry to the sillimanite-bearing horizons but with some higher grossular and lower spessartine contents ($Alm_{52–54}Sps_{16–27}Prp_{10–12}Grs_{11–18}$; Mg# = 0.16–0.18; Table 1). Plagioclase shows a variation of $An_{28–43}$. Biotite has lower values of Mg# (Mg# = 0.44–0.46) and larger variations in Ti (Ti = 0.16–0.40 a.p.f.u.). White mica in the garnet gneiss occurs as well-developed grains reaching some higher Si number (Si = 6.2–6.5).

6 Petrological modelling

To document the metamorphic conditions, equilibrium assemblage diagrams were calculated. The calculations were

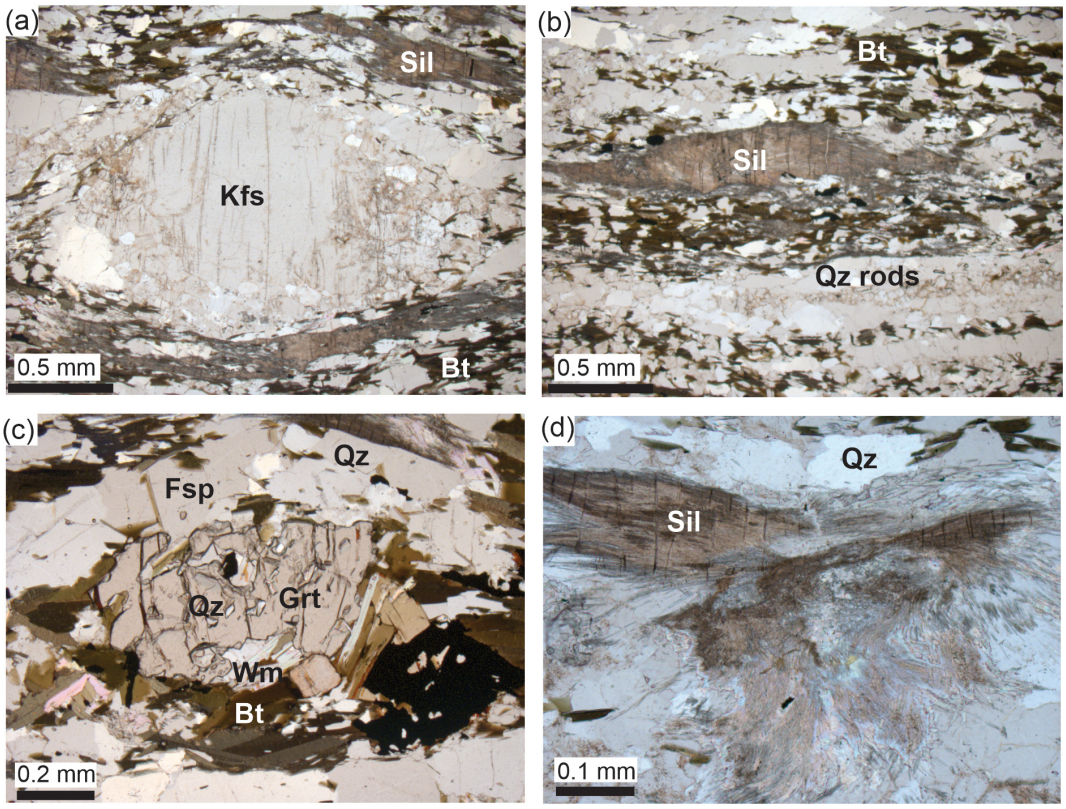

Figure 3. Petrography of sillimanite-bearing gneiss, photomicrographs, plane-polarized light, sample MAN3A (mineral abbreviations after Whitney and Evans, 2010). **(a)** Coarse K-feldspar porphyroblast in sillimanite-rich gneiss matrix. The K-feldspar occurs with an ellipsoidal foliation-parallel shape-preferred orientation with pressure shadows on the long-axis limb. **(b)** Sillimanite porphyroblast in a finer-grained biotite–quartz–feldspar matrix. Foliation is defined by crystal-preferred-orientation micas, elongation and preferred crystal orientation of sillimanite, and a modal banding of phases. Note foliation-parallel quartz rods occurring as < 0.2 mm thick layers. **(c)** Garnet porphyroblasts with irregular grain boundaries in biotite-rich matrix. **(d)** Mass of sillimanite formed by an elongated coarse crystal surrounded by a randomly oriented fibrolitic aggregate.

made using Theriak-Domino computer software (deCapitani and Petrakakis, 2010) with a slightly modified source code (build 011if of 2020 source code, provided by Douglas K. Tinkham on https://dtinkham.net; Thinkham, 2023). The calculations are based on the bulk-rock compositions obtained from the major element XRF analyses (Table 4) and using the internally consistent thermodynamic dataset of Holland and Powell (2011; Theriak-Domino filename td-ds62-mp50-05.txt). The calculations were run in the NCKFMnMASH-TO (Na_2O–CaO–K_2O–FeO–MnO–MgO–Al_2O_3–SiO_2–H_2O–TiO_2) system with H_2O in excess. The modelling has been run for a selection of five samples of garnet–mica and garnet–sillimanite gneisses, and the results are presented for sample MAN3A (Fig. 6), considered representative and relevant.

The presented P–T pseudosection of garnet–sillimanite-bearing gneiss, sample MAN3A, was calculated within the P–T window of 600–800 °C and 0.4–0.9 GPa (Fig. 6a–b). The model results suggest that garnet is stable above 610 °C. Plagioclase is stable up to ca. 730 °C at high pressures and above 800 °C at lower pressures, and K-feldspar is stable up to 665 °C at high pressures and up to ∼ 680 °C at lower pressures. Partial melting occurs at T above ∼ 660 °C at the expense of feldspars and quartz. White mica is stable up to 660–730 °C, biotite breaks down at temperatures above 760–770 °C. The stability of Al silicates is restricted to the temperature field of 660–770 °C, where the high-pressure kyanite polymorph occurs at pressures above 0.8 GPa. According to the pseudosection, the present assemblage including garnet + sillimanite + ilmenite falls within the temperature range of 690–750 °C at pressures up to 0.6 GPa. At this pressure condition of 0.6 GPa, white mica is stable up to 700 °C.

The calculation of garnet isopleths (Fig. 6c–d) gives additional constraints on the P–T conditions. The measured garnet grossular content (core value) ∼ 0.05 (Table 1) indicates pressures of ∼ 0.55–0.60 GPa during the growth of the garnet. Mg# values in the garnet of 0.22–0.23 suggest temperatures of up to 750 °C, in accordance with the upper P–T stability of the assemblage garnet + sillimanite + biotite + feldspar + quartz + ilmenite + melt.

Table 1. Continued.

Rock type	Grt-Sil gneiss			
Sample no.	MAN 9	MAN 9	MAN 9	MAN 9
Analysis no.	2	3	11	20
Comment	core	rim	core	rim
SiO_2	37.89	37.52	37.85	37.55
Al_2O_3	21.47	21.23	21.60	20.99
TiO_2	0.01	0.01	0.00	0.00
Cr_2O_3	0.06	0.03	0.00	0.00
FeO	23.32	20.60	23.36	20.73
MnO	11.33	15.96	11.54	16.10
MgO	5.22	3.33	4.71	3.24
CaO	1.33	1.55	1.77	2.05
Total	100.63	100.23	100.83	100.66
Formula based on eight cations				
Si	2.99	3.00	2.98	3.00
Al	1.99	2.00	2.01	1.97
Ti	0.00	0.00	0.00	0.00
Cr	0.00	0.00	0.00	0.00
Fe^{2+}	1.54	1.38	1.54	1.38
Mn	0.76	1.08	0.77	1.09
Mg	0.61	0.40	0.55	0.39
Ca	0.11	0.13	0.15	0.18
Oxygen	11.98	12.01	11.99	11.98
Alm	50.9	46.1	51.1	45.6
Prp	20.3	13.3	18.4	12.7
Grs	3.7	4.4	5.0	5.8
Sps	25.1	36.2	25.6	35.9
Mg#	0.29	0.22	0.26	0.22

$Alm = (Fe^{2+}/(Fe^{2+} + Mn + Mg + Ca)) \cdot 100$.
$Prp = (Mg/(Fe^{2+} + Mn + Mg + Ca)) \cdot 100$.
$Grs = (Ca/(Fe^{2+} + Mn + Mg + Ca)) \cdot 100$.
$Sps = (Mn/(Fe^{2+} + Mn + Mg + Ca)) \cdot 100$. $Mg\# = Mg/(Mg + Fe)$.

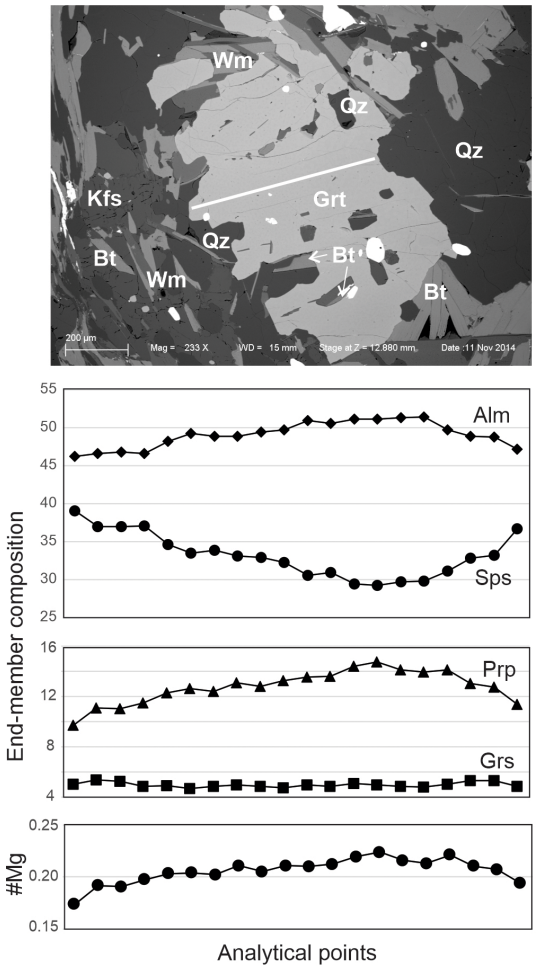

Figure 4. BSE image and garnet zoning profile, sillimanite-bearing augen gneiss, sample MAN3A: garnet is almandine- and spessartine-rich. Inclusions in garnet are constituted by quartz and biotite. Irregular garnet grain boundaries are surrounded by biotite, white mica and quartz. Garnet shows a rimward decrease in almandine, pyrope, and resulting Mg#; a smaller decrease in grossular; and a marked increase in spessartine.

7 Discussion

7.1 Petrological evolution

7.1.1 Record of peak metamorphism?

The rimward decrease in the Mg# (Fig. 4) in the garnet indicates that the core of the garnet formed at the highest recorded temperatures. This is further supported by the relatively homogeneous content of grossular with a slight decrease at the rims. Any preservation of a prograde formation of the garnet cores is not found and can be explained by re-equilibration of its chemistry due to the high peak-metamorphic temperatures (e.g. Caddick et al., 2010). This is in accordance with the presence of inclusions of biotite and quartz in garnet (Fig. 4), phases that are stable together with garnet at the higher pressures and high temperatures of up to 770 °C (Fig. 6).

The pseudosection modelling suggests that the observed metamorphic mineral assemblage of garnet–sillimanite–plagioclase–quartz–biotite in the sillimanite gneiss is stable at P–T conditions up to 750 °C and 0.6 GPa (Fig. 6). The pseudosection modelling further suggests that the high-temperature equilibrium of the sillimanite gneiss was associated with partial melting of the rock, as evidenced by K-feldspar–plagioclase–quartz leucosome pockets (Fig. 2f–g) and pegmatites in outcrop. Elsewhere in the WGR, partial melting has been reported to postdate the (U)HP metamorphism and eclogite formation and was dated at 403–395 Ma (Krogh et al., 2011; Tucker et al., 2004). The $Grt_{Mg\#}$ isopleths are temperature-sensitive and illustrate a maximum temperature of up to 750 °C at the time of equilibration of the garnet (Fig. 6c). Grt_{Grs} isopleths are pressure-sensitive (Fig. 6d) and indicate pressures of 0.6 GPa.

Table 2. Representative electron-microprobe analyses of feldspar (oxide wt%, formula in atoms per formula unit, a.p.f.u.).

Rock type	Grt-mica gneiss		Grt-Sil gneiss		Grt-mica gneiss
Sample no.	MAN2A	MAN2A	MAN3A	MAN3A	MAN4
Analysis no.	10	18	55	66	74
Comment	core	core	core	core	core
SiO_2	57.01	60.66	60.39	60.64	57.37
Al_2O_3	26.44	23.93	24.55	24.40	26.82
CaO	9.12	6.01	6.37	6.17	9.11
Na_2O	6.54	8.12	8.07	8.21	6.55
K_2O	0.25	0.40	0.23	0.18	0.18
FeO	0.07	0.09	0.08	0.07	0.07
Total	99.44	99.20	99.69	99.69	100.10
Formula based on five cations					
Si	2.57	2.72	2.69	2.70	2.57
Al	1.40	1.26	1.29	1.28	1.41
Ca	0.44	0.29	0.30	0.29	0.44
Na	0.57	0.70	0.70	0.71	0.57
K	0.01	0.02	0.01	0.01	0.01
Fe	0.00	0.00	0.00	0.00	0.00
Oxygen	7.98	7.98	7.98	7.98	7.99
An	42.9	28.4	30.0	29.0	43.0
Ab	55.7	69.4	68.7	69.9	55.9
Kfs	1.4	2.2	1.3	1.1	1.1

Table 2. Continued.

Rock type	Grt-Sil gneiss	
Sample no.	MAN 9 II	MAN 9 II
Analysis no.	24	25
Comment	core	rim
SiO_2	58.40	58.40
Al_2O_3	26.43	26.64
CaO	8.62	8.60
Na_2O	6.83	6.85
K_2O	0.27	0.23
FeO	0.08	0.17
Total	100.63	100.87
Formula based on five cations		
Si	2.60	2.59
Al	1.39	1.39
Ca	0.41	0.41
Na	0.59	0.59
K	0.02	0.01
Fe	0.00	0.01
Oxygen	7.99	7.99
An	40.5	40.5
Ab	58.0	58.3
Kfs	1.5	1.2

$An = (Ca/(Ca + Na + K)) \cdot 100.$
$Ab = (Na/(Ca + Na + K)) \cdot 100.$
$Kfs = (K/(Ca + Na + K)) \cdot 100.$

Evidence for a former higher-pressure metamorphism of the gneisses in the area is proved by the presence of eclogite lenses, from which pressures of 1.6–1.8 GPa for the peak eclogite-facies metamorphism have been estimated (Larsen et al., 1998; Walsh and Hacker, 2004; Engvik et al., 2018), implying a post-eclogite-facies decompression evolution of the gneisses prior to the present state. Higher pressures are also supported by the high Si number of white mica up to 6.5 a.p.f.u. of the gneisses (Table 3). The P–T path has most likely crossed the kyanite–sillimanite reaction line during the prograde and/or retrograde evolution. With such a regional decompression evolution in the area (Larsen et al., 1998; Walsh and Hacker, 2004; Engvik et al., 2018; see discussion below), it is debatable whether the texture of the coarse sillimanite porphyroblasts (Fig. 5c–d) with microfractures perpendicular to the cleavage direction has been inherited after kyanite. Both kyanite and sillimanite gneisses are reported in the neighbouring coastal part of WGR (Tveten et al., 1998; March et al., 2022).

7.1.2 Retrogression

The post-eclogite-facies metamorphic evolution can be deduced from the observed mineral textures and fabric involving garnet, plagioclase, K-feldspar, sillimanite, muscovite, quartz and melt in combination with the pseudosection modelling.

The garnet grossular content shows a relatively flat profile but with a decrease in the outer rim of the garnet (Fig. 4). The grossular decrease in the garnet rims is interpreted as a

Table 3. Representative electron-microprobe analyses of sheet silicates (oxide wt %, formula in atoms per formula unit, a.p.f.u.).

Rock type	Grt-mica gneiss				Grt-Sil gneiss	
Sample no.	MAN2A	MAN2A	MAN2A	MAN2A	MAN3A	MAN3A
Analysis no.	4	17	8	15	53	64
Mineral	White mica	White mica	Biotite	Biotite	White mica	White mica
SiO_2	45.19	45.28	34.57	34.96	45.14	45.04
Al_2O_3	31.97	32.39	16.48	16.86	33.46	33.41
TiO_2	0.40	0.22	3.35	3.47	1.10	0.91
Cr_2O_3	0.04	0.01	0.04	0.03	0.00	0.02
FeO	4.54	3.75	20.19	19.92	3.26	3.47
MnO	0.05	0.03	0.57	0.45	0.04	0.03
MgO	1.42	0.97	8.94	8.88	0.68	0.70
CaO	0.00	0.00	0.00	0.00	0.00	0.00
Na_2O	0.32	0.55	0.11	0.14	0.43	0.45
K_2O	10.98	10.85	9.81	9.85	10.68	10.73
Total	94.90	94.04	94.06	94.55	94.78	94.76
Formula based on 22 O						
Si	6.18	6.22	5.42	5.43	6.13	6.12
Al	5.15	5.24	3.04	3.09	5.35	5.35
Ti	0.04	0.02	0.39	0.40	0.11	0.09
Cr	0.00	0.00	0.01	0.00	0.00	0.00
Fe^{2+}	0.52	0.43	2.65	2.59	0.37	0.40
Mn	0.01	0.00	0.08	0.06	0.00	0.00
Mg	0.29	0.20	2.09	2.06	0.14	0.14
Ca	0.00	0.00	0.00	0.00	0.00	0.00
Na	0.08	0.15	0.03	0.04	0.11	0.12
K	1.92	1.90	1.96	1.95	1.85	1.86
Cations	14.20	14.16	15.66	15.62	14.06	14.09
Mg#			0.44	0.44		

response to decompression (Fig. 6d). The Mg# shows some larger variations through the garnet, but its corresponding rimward decrease reflects retrogression, i.e. a decrease in the metamorphic temperatures. The embayed garnet rims indicate resorption during retrogression (Fig. 3c). The resorbed garnet rims are in equilibrium with biotite, white mica and quartz, indicating a retrogression below 700 °C, according to the garnet + white mica stability fields in the modelled pseudosection (Fig. 6a–b).

Any fractionation of the bulk chemistry, potentially due to garnet growth, could have an effect on the P–T modelling (Gaidies et al., 2008; Faryad and Ježek, 2019). However, fractionation is assumed low, as garnet occurs only in minor modal amounts in the sillimanite gneiss, and its chemical zoning is minor, within Mg# = 0.07 and with only minor changes in grossular content. The high spessartine content of the garnet cores (up to 29 mol %, Table 1) is characteristic of the sillimanite-bearing gneisses, in contrast to garnet in the regional eclogites, HP granulites and country-rock gneisses, which show $Grt_{Sps} \leq 3$ (Walsh and Hacker, 2004; Engvik et al., 2018). The rimward spessartine increase can be explained by the resorption; as garnet is the major Mn-bearing phase in the gneiss assemblage, dissolved Mn will need to be incorporated into the host garnet.

According to pseudosection modelling, field relations and petrographic textures, the phase relations between feldspars, sillimanite, white mica and melt are complex. Figures 2a, 3a and 5a show sillimanite associated with the K-feldspar porphyroclasts. The textures of Fig. 5c–d illustrate a replacement of sillimanite by white mica and quartz, which corresponds to the coherence of the reaction lines of sillimanite-out and white mica-in in the calculated pseudosection during retrogression (Fig. 6a–b). The assemblage is observed to be stable with biotite, which is in accordance with the calculated pseudosection. Very fine-grained aggregates of sillimanite, quartz and white mica surrounding remnants of K-feldspar (Fig. 5b) illustrate the replacement reaction:

$$\text{K-feldspar} + \text{sillimanite} + \text{water} = \text{muscovite} + \text{quartz}$$

$$KAlSi_3O_8 + Al_2SiO_5 + H_2O = KAl_2(AlSi_3O_{10})(OH)_2 + SiO_2.$$

The replacement textures in Fig. 5 also illustrate the metastability of K-feldspar and that the reaction requires water to replace K-feldspar. The pseudosection gives complex

Table 3. Continued.

Rock type	Grt-Sil gneiss		Grt-mica gneiss	
Sample no.	MAN3A	MAN3A	MAN4	MAN4
Analysis no.	50	68	77	71
Mineral	Biotite	Biotite	White mica	Biotite
SiO_2	35.29	35.27	47.76	35.11
Al_2O_3	17.96	18.32	29.72	17.53
TiO_2	3.14	2.78	0.70	1.37
Cr_2O_3	0.00	0.00	0.03	0.03
FeO	18.23	17.49	3.21	20.40
MnO	0.70	0.56	0.03	0.46
MgO	9.46	10.29	1.76	9.70
CaO	0.00	0.00	0.02	0.01
Na_2O	0.10	0.12	0.27	0.12
K_2O	9.83	9.71	10.80	9.78
Total	94.71	94.54	94.29	94.51
Formula based on 22 O				
Si	5.41	5.39	6.50	5.46
Al	3.25	3.30	4.77	3.21
Ti	0.36	0.32	0.07	0.16
Cr	0.00	0.00	0.00	0.00
Fe^{2+}	2.34	2.24	0.37	2.65
Mn	0.09	0.07	0.00	0.06
Mg	2.17	2.35	0.36	2.25
Ca	0.00	0.00	0.00	0.00
Na	0.03	0.03	0.07	0.04
K	1.92	1.89	1.88	1.94
Cations	15.58	15.60	14.02	15.77
Mg#	0.48	0.51		0.46
Rock type	Grt-Sil gneiss			
Sample no.	MAN 9	MAN 9	MAN 9	MAN 9 II
Analysis no.	6	8	18	22
Mineral	White mica	White mica	Biotite	Biotite
SiO_2	45.39	46.61	36.29	35.68
Al_2O_3	34.45	32.33	18.49	17.70
TiO_2	0.44	0.29	1.44	2.89
Cr_2O_3	0.00	0.01	0.00	0.02
FeO	3.04	2.74	15.96	18.65
MnO	0.08	0.06	0.62	0.47
MgO	0.97	1.44	12.33	9.99
CaO	0.00	0.00	0.00	0.00
Na_2O	0.37	0.35	0.08	0.11
K_2O	10.87	10.90	10.01	9.77
Total	95.56	94.65	95.18	95.27
Formula based on 22 O				
Si	6.10	6.31	5.46	5.44
Al	5.46	5.16	3.28	3.18
Ti	0.04	0.03	0.16	0.33
Cr	0.00	0.00	0.00	0.00
Fe^{2+}	0.34	0.31	2.01	2.38
Mn	0.01	0.01	0.08	0.06
Mg	0.19	0.29	2.77	2.27
Ca	0.00	0.00	0.00	0.00
Na	0.10	0.09	0.02	0.03
K	1.86	1.88	1.92	1.90
Cations	14.11	14.07	15.71	15.60
Mg#			0.58	0.49

$Mg\# = Mg/(Mg + Fe)$.

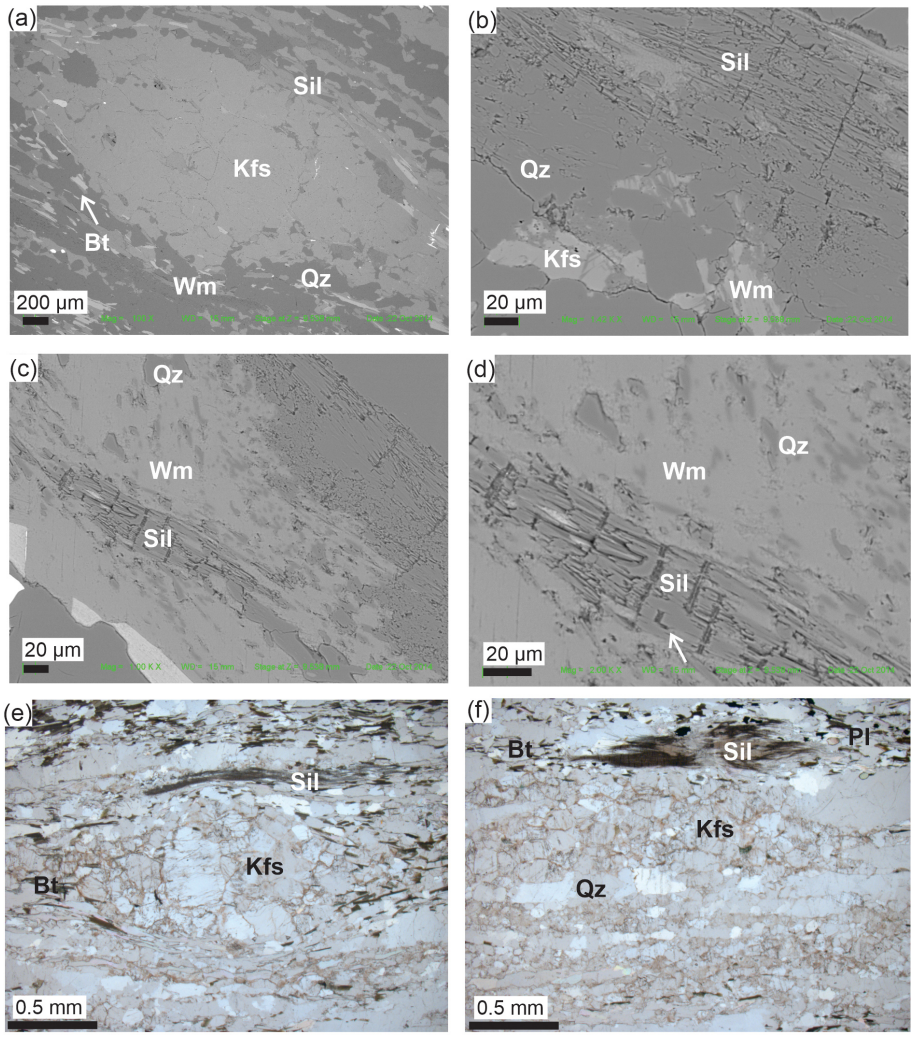

Figure 5. Replacement textures of sillimanite-bearing gneiss, sample MAN3A. **(a)** Coarse K-feldspar porphyroclast in the well-foliated fabric of quartz, K-feldspar and biotite. Rims of the coarse K-feldspar show replacement by fine grains of sillimanite, quartz and white mica. BSE image. **(b)** Detail of K-feldspar porphyroclast margin showing replacement by an aggregate of sillimanite–quartz–white-mica–K-feldspar. BSE image. **(c)** Aggregate of white mica and quartz occurs together with sillimanite. BSE image. **(d)** Close-up from panel **(c)**. Note sillimanite microfractures perpendicular to the sillimanite elongation and cleavage direction. BSE image. **(e)** K-feldspar porphyroblasts composed of a monomineralic medium-grained aggregate. Photomicrograph, plane-polarized light. **(f)** Foliated heterogranular sillimanite gneiss with fine-grained matrix of quartz, plagioclase, K-feldspar and biotite, including a modal biotite banding of the gneiss. Photomicrograph, plane-polarized light.

relationships on feldspar stability (Fig. 6a–b). According to the modelling, K-feldspar is stable up to 660 °C, at lower pressures up to 680 °C, even in the presence of melt (field 3 in Fig. 6a). The local preservation of perthite in the porphyroclasts illustrates its metastable preservation as remnant from a higher-temperature stage. Plagioclase is stable up to ca. 730 °C at high pressures and above 800 °C at lower pressures. White mica is stable together with sillimanite at temperatures of 680–700 °C. This is below the recorded peak-metamorphic temperature of ∼ 750 °C but approaches the field with the peak-metamorphic mineral assemblage garnet + sillimanite + biotite + plagioclase + quartz + ilmenite + melt.

The pseudosection modelling assumes a closed system and full equilibration. However, mineral replacement reactions involve the exchange of elements and a variable fluid chemistry, as transformation by alkali leaching (McLelland et al., 2002), and give a possible metasomatic environment for which the model based on a chemical closed system will not be fully representative. Mass transport of partially melted material will similarly cause a change in stability. The partial melting, starting at temperature above 660 °C, occurs at the expense of quartz and feldspar. Field relations including

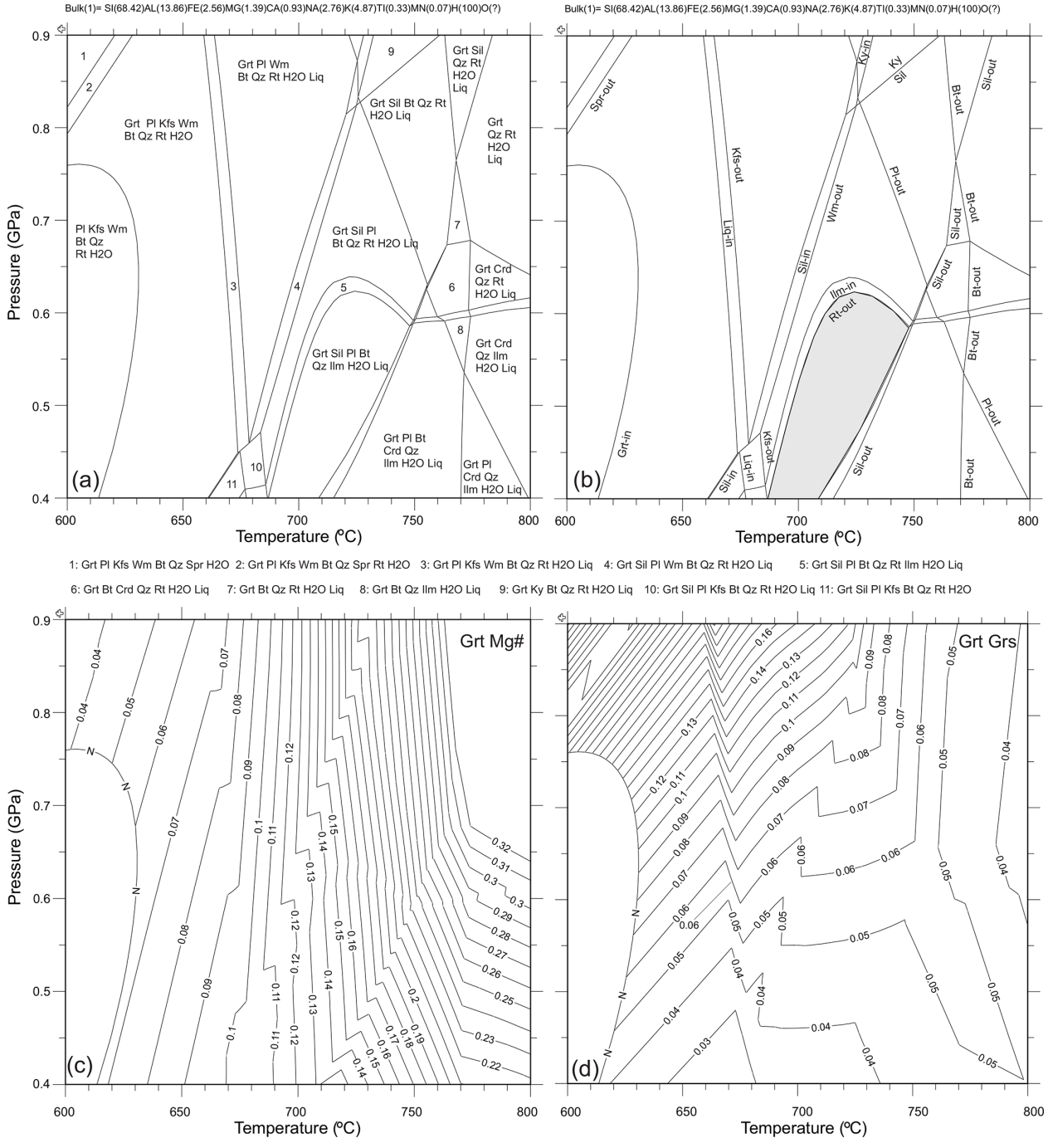

Figure 6. P–T pseudosections calculated by Theriak-Domino software, sample MAN3A; see text for discussion. Solution models are selected by the software with the database td-ds62-mp50-05.txt: H2O, PS94H2O. STLP, site mixing + margules. MIN, site mixing + margules. PREH, site mixing + margules. PMP, site mixing. GRT, site mixing + margules. LIQtc6, external + margules. FSP4TR, site mixing + margules. ABHGP, site mixing + margules. EP11, site mixing + margules. MRG, site mixing + margules. WM, site mixing + margules. BI14, site mixing + margules. OPX14, site mixing + margules. SAPP, site mixing + margules. CD14, site mixing + margules. ST14, site mixing + margules. CHL14, site mixing + margules. CTD14, site mixing + margules. MTLOW, site mixing + margules. ILM00, site mixing + margules. **(a)** Stability fields with mineral assemblage. **(b)** Mineral in–out reactions. Grey area represents the stability field with the mineral assemblage observed. **(c)** Compositional isopleths of garnet Mg#. **(d)** Compositional isopleths of grossular in garnet.

Table 4. Whole-rock analysis (wt %).

Rock type	Grt-Sil gneiss
Sample no.	MAN3A
SiO_2	73.90
Al_2O_3	12.70
Fe_2O_{3total}	3.67
TiO_2	0.48
MgO	1.01
CaO	0.94
Na_2O	1.54
K_2O	4.12
MnO	0.09
P_2O_5	0.06
LOI	0.78
Total	99.30

migmatitic parts with leucosomes and quartz–feldspar veins illustrate the local presence of voluminous melt.

7.1.3 Microfabric evolution

The coarse K-feldspar porphyroclasts show an ellipsoidal form with foliation-aligned pressure shadows and fine-grained mineral replacements along their rims (Figs. 3b and 4a). The foliation comprising biotite and sillimanite wraps around the K-feldspar porphyroclasts. These porphyroclasts are replaced by subgrains (Fig. 5e) but still show the characteristic foliation-parallel pressure shadows and are surrounded by undulating foliation of oriented biotite and sillimanite crystals. Monomineralic layers of fine-grained (0.2 mm) K-feldspar (Figs. 3a and 5e) are interpreted as deformed, elongated and granulated large former K-feldspar porphyroclast (Figs. 2a and 5e–f).

Rheological experiments have shown that a higher creep strength of relatively dry K-feldspar compared to wet quartzite provides an explanation for feldspar forming porphyroclasts in crustal rocks (Chen et al., 2021). This can also explain that quartz occurs in monomineralic foliation-parallel rods comprising finer grains of $> 0.1 \times 0.5$ mm in the sillimanite gneiss (Fig. 3b). Development of elongate quartz aggregates (type B quartz ribbons, according to Boullier and Bouchez, 1978), like those observed here, is commonly interpreted by flattening and/or stretching of single quartz grains or aggregates and/or coalescence of grains involving deformation by dislocation glide and grain boundary migration at upper amphibolite to granulite facies conditions (e.g. Mandal et al., 1997; Hippertt et al., 2001; Engvik et al., 2020). The recorded mineral replacements by K-feldspar subgrain formation, formation of quartz rods, coarse foliation-parallel sillimanite crystals and garnet porphyroclasts, all constituting the present well-developed gneiss foliation, are interpreted to have formed during the decompression and retrogression stage.

7.2 Regional implications

Vernon (1990) argued that K-feldspar augen and megacrysts in felsic gneisses and mylonites are generally residual phenocrysts, i.e. representing variably deformed megacrysts from former granitoids rather than porphyroblasts. Although the presence of sillimanite is usually suggesting a sedimentary rock origin (e.g. Spry et al., 2022), the findings of Vernon (1990) seem relevant to the regional setting in Romsdal, where K-feldspar occurs as augen in lithologies mapped as granitoid gneisses (Tveten et al., 1998). Other studies assigning the origin of sillimanite-bearing gneisses to a granitoid environment include Nabelek (1997) and McLelland et al. (2002).

In the Romsdal area, sillimanite gneisses occur interlayered with eclogite-facies metamorphic rocks. The two lithologies preserve metamorphic mineral assemblages formed at different conditions, i.e. high-temperature granulite facies versus high-pressure eclogite facies. Eclogite in the Romsdal area equilibrated, according to Walsh and Hacker (2004), at 650–800 °C and 1.6–1.8 GPa, i.e. at considerable higher pressures than the sillimanite-bearing gneisses studied here. The differences in the development of preserved metamorphic mineral assemblages might be explained by equilibration and deformation at different stages during the metamorphic cycles. Eclogites testify to the high-pressure stage during burial to great depths in an orogenic cycle. The P–T estimates derived from the eclogite mineral assemblages are usually interpreted as the peak-metamorphic stage. In the adjacent coastal Møre and Romsdal area, the preserved garnet–clinopyroxene rock recorded metamorphism of high-pressure granulite facies estimated to > 900 °C and 1.4–1.8 GPa (Engvik et al., 2018) and 875–970 °C and 1.32–1.45 GPa (Holmberg et al., 2019). The high-pressure granulite is interpreted as a decompression stage after a former higher-pressure eclogite-facies metamorphism. Larsen et al. (1998) reported similar granulite-facies conditions of 1.6–2.3 GPa and T up to 800 °C following the eclogite-facies stage with a clockwise trajectory including isothermal decompression from high pressures. In the Romsdal area, situated E/SE of the above-referred works, the peak-metamorphic temperatures and pressures are lower according to the regional model and datasets by Krogh (1977) and Hacker et al. (2010). The postulated northwestward increase in pressures and temperatures may explain the better preservation of the eclogite-facies assemblages in the northwestern Romsdal area (Walsh and Hacker, 2004).

The above-presented observed mineral assemblages and replacement reactions that resulted in the formation of the present-day well-developed gneiss foliation are interpreted to have formed during the decompression and retrogression stage. This is in accordance with the observed microfabric evolution with a well-developed foliation and fabric including crystal-preferred orientation of sillimanite and mica, as well as K-feldspar subgrain formation, quartz rod evolution

and its development to foliation-parallel felsic layers. This fabric development is interpreted as a continuous decompression and retrogression evolution, also in accordance with the interpretations from Engvik et al. (2018) and Larsen et al. (1998) from the adjacent coastal area. The regional high-pressure setting and local preservation of eclogite lenses and layers in close relation to the sillimanite gneisses can be explained by differences in the availability of fluids and melt during metamorphic evolution. Water reactions with K-feldspar and sillimanite forming white mica enhanced deformation and crossing of the liquidus of the felsic/granitoid lithology when T increased above $\sim 670\,^{\circ}\mathrm{C}$ (Fig. 6), whereas the mafic lithologies recording eclogite-facies metamorphism did, locally, not fully equilibrate during retrogression. This context and processes can explain the close spatial field relationships between sillimanite gneiss and eclogite.

8 Conclusions

This work documents the presence, composition, formation and metamorphic evolution of sillimanite-bearing gneisses in the Romsdal region of the Western Gneiss Region (south Norway).

- Sillimanite occurs in augen gneiss, constituting nuggets in so-called nodular gneiss, and is present in well-foliated sillimanite–mica gneiss. Lenses and layers of eclogite occur within the sillimanite-bearing units.

- The sillimanite-bearing gneisses are heterogranular with a matrix dominated by quartz, plagioclase ($An_{29–41}$), K-feldspar, biotite (Mg# = 0.48–0.58; Ti = 0.16–0.36 a.p.f.u.) and variable amounts of white mica (Si = 6.1–6.3). K-feldspar occurs as porphyroclasts in augen gneisses, and garnet occurs as resorbed porphyroblasts. Garnet ($Alm_{46–56}$ $Sps_{24–36}Prp_{10–20}Grs_{4–6}$; Mg# = 0.22–0.29) shows rimward-decreasing Mg# and grossular values, as well as a marked rimward spessartine increase up to Sps_{36}.

- Foliation is defined by crystal-preferred-orientation micas, elongation of shape-preferred-orientation coarse K-feldspar phenocrysts and a modal banding of phases. The ellipsoidal foliation-parallel K-feldspar porphyroclasts show pressure shadows on the long-axis limb. Sillimanite occurs as coarse parallel-oriented matrix porphyroblasts, as finer grains and as fibrolitic aggregates constituting very fine-grained radiating crystals. Quartz forms coarser elongated grains and monomineralic rods.

- Pseudosection modelling suggests that the peak assemblage of garnet–sillimanite–feldspar–biotite–quartz–ilmenite–melt equilibrated at temperatures up to 750 °C and pressures of 0.6 GPa.

- Subsequent retrogression, which consumed garnet, indicates mineral replacement and melt crystallization involving sillimanite, white mica, K-feldspar and quartz.

The petrological, mineral chemical and microfabric observations indicate a decompression and document a retrogressive evolution of the sillimanite gneisses in accordance with the investigated eclogites and high-pressure granulites in this northwestern part of Western Gneiss Region.

Data availability. Data are available upon request.

Author contributions. AKE designed this study, including conceptualization, geological field studies and sampling, petrography, analytical work, and writing. JJ ran pseudosection modelling and contributed to the interpretation of data and writing.

Competing interests. The contact author has declared that neither of the authors has any competing interests.

Disclaimer. Publisher's note: Copernicus Publications remains neutral with regard to jurisdictional claims made in the text, published maps, institutional affiliations, or any other geographical representation in this paper. While Copernicus Publications makes every effort to include appropriate place names, the final responsibility lies with the authors.

Special issue statement. This article is part of the special issue "(Ultra)high-pressure metamorphism, from crystal to orogenic scale". It is a result of the 14th International Eclogite Conference (IEC-14) held in Paris and Lyon, France, 10–13 July 2022.

Acknowledgements. This work is supported by the Geological Survey of Norway. We thank Åknes/Tafjord Beredskap IKS for access to drill cores from the Mannen massif in Romsdalen; Ole Lutro, Øystein Nordgulen and Synnøve Elvevold for discussions on the Romsdal gneisses; and Anne Liinamaa-Dehls for improving the English language of the paper. We are thankful to two anonymous referees whose constructive criticism has improved the paper.

Review statement. This paper was edited by Samuel Angiboust and reviewed by two anonymous referees.

References

Andersen, T. B., Jamtveit, B., Dewey, J. F., and Swensson, E.: Subduction and eduction of continental crust: major mechanisms during continent-continent collision and orogenic extensional collapse, a model based on the south Caledonides, Terra Nova, 3, 303–310, 1991.

Austrheim, H., Corfu, F., Bryhni, I., and Andersen, T. B.: The Proterozoic Hustad igneous complex; a low strain enclave with a key to the history of the Western Gneiss Region of Norway, Precambrian Res., 120, 149–175, 2003.

Barrow, G.: On the geology of lower Dee-side and the southern Highland Border, P. Geologist. Assoc., 23, 274–290, 1912.

Boullier, A.-M. and Bouchez, J.-L.: Le quartz en rubans dans les mylonites, B. Soc. Géol. Fr., 7, 253–262, 1978.

Butler, J. P., Jamieson, R. A., Steenkamp, H. M., and Robinson, P.: Discovery of coesite-eclogite from Nordøyane UHP domain, Western Gneiss Region, Norway: field relations, metamorphic history, and tectonic significance, J. Metamorph. Geol., 31, 147–163, 2013.

Caddick, M. J., Konopasek, J., and Thompson, A. B.: Preservation of Garnet Growth Zoning and the Duration of Prograde Metamorphism, J. Petrol., 51, 2327–2347, 2010.

deCapitani, C. and Petrakakis, K.: The computation of equilibrium assemblage diagrams with Theriak/Domino software, Am. Mineral., 95, 1006–1016, 2010.

Chen, J., Jin, Z., Liu, W., Wang, Y., and Jufeng, Z.: Rheology of dry K-feldspar aggregate at high temperature and high pressure: An experimental study, Tectonophysics, 817, 229072, https://doi.org/10.1016/j.tecto.2021.229072, 2021.

DesOrmeau, J. W., Gordon, S. M., Kylander-Clark, A. R. C., Hacker, B. R., Bowring, S. A., Schoene, B., and Samperton, K. M.: Insights into (U)HP metamorphism of the Western Gneiss Region, Norway: A high-spatial resolution and high-precision zircon study, Chem. Geol., 414, 138–155, 2015.

Dobrzhinetskaya, L. F., Eide, E. A., Larsen, R. B., Sturt, B. A., Trønnes, R., Smith, D. C., Taylor, W. R., and Posukhova, T. V.: Microdiamond in high-grade metamorphic rocks of the Western Gneiss Region, Norway, Geology, 7, 597–600, 1995.

Engvik, A. K. and Andersen, T. B.: Evolution of Caledonian deformation fabrics under eclogite and amphibolite facies at Vårdalsneset, Western Gneiss Region, Norway, J. Metamorph. Geol., 18, 241–257, 2000.

Engvik, A. K., Austrheim, H., and Andersen, T. B.: Structural, mineralogical and petrophysical effects on deep crustal rocks of fluid-limited polymetamorphism, Western Gneiss Region, Norway, J. Geol. Soc. Lond., 157, 121–134, 2000.

Engvik, A. K., Willemoes-Wissing, B., and Lutro, O.: High-temperature, decompressional equilibration of the eclogite facies orogenic root, Western Gneiss Region, Norway, J. Metamorph. Geol., 36, 529–545, 2018.

Engvik, A. K., Mertens, C., and Trepmann, C. A.: Episodic deformation and reactions in mylonitic high-grade metamorphic granulites from Dronning Maud Land, Antarctica, J. Struct. Geol., 141, 104196, https://doi.org/10.1016/j.jsg.2020.104196, 2020.

Faryad, S. W. and Ježek, J.: Compositional zoning in garnet and its modification by diffusion during pressure and temperature changes in metamorphic rocks; an approach and software, Lithos, 332–333, 287–295, 2019.

Gaidies, F., de Capitani, C., and Abart, R.: THERIA_G: a software program to numerically model prograde garnet growth, Contrib. Mineral. Petr., 155, 657–671, 2008.

Gillen, C.: Metamorphic Geology, George Allen & Unwin, London, 1982.

Griffin, W. L., Austrheim, H., Braasted, K., Bryhni, I., Krill, A. G., Krogh, E. J., Mørk, M. B. E., Quale, H., and Tørudbakken, B.: High-pressure metamorphism in the Scandinavian Caledonides, in: The Caledonide Orogen – Scandinavia and Related Areas, edited by: Gee, D. G., and Sturt, B. A., John Wiley & Sons Ltd, Chichester, 783–802, 1985.

Hacker, B. R.: Ascent of the ultrahigh-pressure Western Gneiss Region, Norway, Geol. Soc. Am. Spec. Pap., 419, 171–184, 2007.

Hacker, B. R., Andersen, T. B., Kylander-Clark, A. R. C., Johnston, S., Peterman, E., Walsh, E. O., and Young, D.: High-temperature deformation during continental-margin subduction and exhumation: The ultrahigh-pressure Western Gneiss Region of Norway, Tectonphysics, 480, 149–171, 2010.

Hippertt, J., Rocha, A., Lana, C., Egydio-Silva, M., and Takeshita, T.: Quartz plastic segregation and ribbon development in high-grade striped gneisses, J. Struct. Geol., 23, 67–80, 2001.

Holland, T. J. B. and Powell, R.: An improved and extended internally consistent thermodynamic dataset for phases of petrological interest, involving a new equation of state for solids, J. Metamorph. Geol., 29, 333–383, 2011.

Holmberg, J., Bukala, M., Jeanneret, P., Klonowska, I., and Majka, J.: Decompressional equilibration of the Misund granulite from Otrøy, Western Gneiss Region, Norway, Geol. Carpath., 70, 471–482, 2019.

Krogh, E. J.: Evidence for a Precambrian continent-continent collision in western Norway, Nature, 267, 17–19, 1977.

Krogh, T. E., Kamo, S. L., Robinson, P., Terry, M. P., and Kwok, K.: U-Pb zircon geochronology of eclogites from the Scandian Orogen, Northern Western Gneiss Region, Norway: 14–20 million years between eclogite crystallization and return to amphibolite facies conditions, Can. J. Earth Sci., 48, 441–472, 2011.

Larsen, R. B., Eide, E. A., and Burke, E. A. J.: Evolution of metamorphic volatiles during exhumation of microdiamond-bearing granulites in the Western Gneiss Region, Norway, Contrib. Mineral. Petr., 133, 106–121, 1998.

March, S., Hand, M., Tamblyn, R., Carvalho, B. B., and Clark, C.: A diachronous record of metamorphism in metapelites of the Western Gneiss Region, Norway, J. Metamorph. Geol., 40, 1121–158, 2022.

Mandal, N., Fujino, K., and Samanta, S. K.: Development of quartz ribbons in quartzofeldspathic granulites, P. Indian A.S.-Earth, 106, 225–236, 1997.

McLelland, J., Morrison, J., Selleck, B., Cunningham, B., Olson, C., and Schmidt, K.: Hydrothermal alteration of late- to post-tectonic Lyon Mountain granitic Gneiss, Adirondack Mountains, New York: Origin of quartz-sillimanite segregations, quartz-albite lithologies, and associated Kiruna-type low-Ti Fe-oxide deposits, J. Metamorph. Geol., 20, 175–190, 2002.

Martin, C., Duchene, S., Luais, B., Goncalves, P., Deloule, E., and Fournier, C.: Behavior of trace elements in relation to Lu-Hf and Sm-Nd geochronometers during metamorphic dehydration-hydration in the HP domain of Vårdalsneset, Western Gneiss Region, Norway, Contrib. Mineral. Petr., 159, 437–458, 2010.

Munz, I. A., Wayne, D., and Austrheim, H.: Retrograde fluid infiltration in the high-grade Modum Complex, South Norway; evidence for age, source and REE mobility, Contrib. Mineral. Petr., 116, 32–46, 1994.

Nabelek, P. I.: Quartz-sillimanite leucosomes in high grade schist, Black Hills, South Dakota: a perspective on the mobility of aluminium in high grade metamorphic rocks, Geology, 25, 995–998, 1997.

Oppikofer, T., Bunkholt, H., Ganerød, G. V., and Engvik, A. K.: Mannen unstable rock slope (Møre and Romsdal): Geological and engineering geological logging of drill core KH-02-11 & grain size distribution and XRD analyses of fine-grained breccias, Norges geologiske undersøkelse, NGU Report 2012.036, 2012.

Pouchou, J. P. and Pichoir, F.: Cameca PAP program, Rech. Aerospatiale, 3, 167–192, 1984.

Roberts, D.: The Scandinavian Caledonides: event chronology, palaeogeographic settings and likely modern analogues, Tectonophysics, 365, 283–299, 2003.

Røhr, T. S., Bingen, B., Robinson, P., and Reddy, S. M.: Geochronology of Palaeoproterozoic augen gneisses in the Western Gneiss Region, Norway: evidences for Sveconorwegian zircon neocrystallization and Caledonian zircon deformation, J. Geol., 121, 105–128, 2012.

Saintot, A., Elvebakk, H., Ganerød, G. V., Oppikofer, T., and Farsund, T.: Mannen unstable rock-slope (Romsdal, Møre & Romsdal County): Logging of drill hole and core KH-01-10 coupled to the geomorphologic interpretation of 1 m resolution digital elevation model and terrestrial lidar scan displacement analysis, Norges geologiske undersøkelse, NGU Report 2011.026, 2011.

Smith, D. C.: Coesite in clinopyroxene in the Caledonides and its implications for geodynamics, Nature, 310, 641–644, 1984.

Spry, P. G., Mcfadden, S., Teale, G. S., Alers, B., Shalloe, J. M., and Glenn, J. M.: Nodular sillimanite rocks as field indicators to metamorphosed massive sulphide deposits, Ore Geol. Rev., 141, 104632, https://doi.org/10.1016/j.oregeorev.2021.104632, 2022.

Terry, M. P., Robinson, P., Hamilton, M. A., and Jercinovic, M. J.: Monazite geochronology of UHP and HP metamorphism, deformation, and exhumation, Nordøyane, Western Gneiss Region, Norway, Am. Mineral., 85, 1651–1664, 2000.

Thinkham, D. K.: Dr. Douglas K. Tinkham, Overview, https://dtinkham.net last access: 19 June 2023.

Tucker, R. D., Råheim, A., Krogh, T. E., and Corfu, F.: Uranium-lead zircon and titanite ages from the northern portion of the Western Gneiss Region, south-central Norway, Earth Planet. Sc. Lett., 81, 203–211, 1987.

Tucker, R. D., Robinson, P., Solli, A., Gee, D. G., Thorsnes, T., Krogh, T. E., Nordgulen, Ø., and Bickford, M. E.: Thrusting and extension in the Scandinavian hinterland, Norway: New U-Pb ages and tectonostratigraphic evidences, Am. J. Sci., 304, 477–532, 2004.

Tveten, E., Lutro, O., and Thorsnes, T.: Geologisk kart over Noreg: berggrunnskart Ålesund: M 1 : 250.000, Norges geologiske undersøkelse, 1998.

Vernon, R. H.: Formation of late sillimanite by hydrogen metasomatism (base leaching) in some high-grade gneisses, Lithos, 12, 143–145, 1979.

Vernon, R. H.: K-feldspar augen in felsic gneisses and mylonites – deformed phenocrysts or porphyroblasts?, GFF, 112, 157–167, 1990.

Vrijmoed, J. C., Van Roermund, H. L. M., and Davies, G.: Evidence for diamond-grade ultra-high pressure metamorphism and fluid interaction in the Svartberget Fe-Ti garnet periodotite-websterite body, Western Gneiss Region, Norway, Miner. Petrol., 88, 381–405, 2006.

Wain, A. L.: New evidence for coesite in eclogite and gneisses: Defining an ultrahigh-pressure province in the Western Gneiss region of Norway, Geology, 25, 927–930, 1997.

Walsh, E. O. and Hacker, B. R.: The fate of subducted continental margins: Two-stage exhumation of the high-pressure to ultrahigh-pressure Western Gneiss Region, Norway, J. Metamorph. Geol., 22, 671–687, 2004.

Walsh, E. O., Hacker, B. R., Gans, P. R., Grove, M., and Gehrels, G.: Protolith ages and exhumation histories of (ultra)high-pressure rocks across the Western Gneiss Region, Norway, Geol. Soc. Am. Bull., 119, 289–301, 2007.

Walsh, E. O., Hacker, B. R., Gans, P. B., Wong, M. S., and Andersen, T. B.: Crustal exhumation of the Western Gneiss Region UHP terrane, Norway: $^{40}Ar/^{39}Ar$ thermochronology and fault-slip analysis, Tectonophysics, 608, 1159–1179, 2013.

Whitney, D. L. and Evans, B. W.: Abbreviations for names of rock-forming minerals, Am. Mineral., 95, 185–187, 2010.